# Proximity-Induced Colossal Conductivity Modulation in Phosphorene

A. Chaudhury, S. Majumder, and S. J. Ray*
*Department of Physics, Indian Institute of Technology Patna, Bihta 801106, India*

(Received 19 June 2018; revised manuscript received 23 November 2018; published 22 February 2019)

Phosphorene is a promising single-elemental two-dimensional layered semiconductor with huge potential for future nanoelectronics and spintronics applications. In this work, we investigate the effect of an organic molecule (benzene) in the close proximity of a phosphorene nanoribbon. Our extensive calculations reveal that the semiconducting nature of phosphorene remains unaffected as a result of the molecular adsorption while the transport properties go through drastic changes. Under the influence of dopant atoms and external strain, colossal changes in the conductivity are observed, with a maximum enhancement $>1500\%$. This effect is pretty robust against (i) variation of the system size, (ii) the type, location, and concentration of dopants and (iii) the nature and magnitude of the external strain. Furthermore, we demonstrated how a gate voltage can be used to fine tune the enhanced conductivity response in a field-effect transistor (FET) structure. Our results provide direction for phosphorene-based nanoelectronics in applications such as sensing, switching where a higher level of conduction can offer better resolution, a higher on:off ratio, and superior energy efficiency.

DOI: 10.1103/PhysRevApplied.11.024056

## I. INTRODUCTION

Two-dimensional (2D) layered structures are crystalline nanomaterials with superior electronic, optical, and mechanical properties that have potential applications in future nanoelectronics and spintronics [1]. Doping in such materials is commonly used for tuning the band gap and electronic properties, the design of high-performance sensors, *p*-*n* junctions, enhancement of the conductivity in FET structures, etc., while the presence of various transition-metal atoms can offer ferromagnetic functionalities and diverse magnetic ground states that are useful in the design of various spintronic devices. Among the recently discovered 2D materials, phosphorene is anticipated to be a preferred candidate over graphene and transition-metal dichalcogenides for future nanoelectronics, as it uniquely offers ambipolar transport [2], high carrier mobility [3], a large on:off ratio [4,5], a tuneable band gap, and low spin-orbit coupling [6,7]. Additionally, the application of strain on phosphorene results in conduction anisotropy [8–10], phase transition [9,11–15], a tuneable Young's modulus [16], a negative Poisson's ratio [17], band-gap engineering [11,15,18–26], Dirac-like cones [27,28], etc., which offers a new way to manipulate the structure as per the specific requirement. Owing to these excellent attributes, intense research in phosphorene is in full swing, to look for new phenomena and applications, which continue to fascinate scientists and technologists.

Due to the enhanced surface-to-volume ratio, 2D materials are sensitive to the presence of a neighboring molecule, as demonstrated in graphene [29] and carbon-nitrogen compounds [30]. The adsorption process results in charge transfer between the molecule and the host layer, leading to an enhanced conduction. From a nanoelectronic perspective, enhanced conduction is highly desirable in the design of field-effect transistors (FETs) or similar switching elements [31–33], where the increase in the "on" current can significantly improve the on:off ratio and the switching performance. Due to constant-size scaling in the complementary metal oxide semiconductor (CMOS) architecture, the presence of leakage current is a major issue of concern. Enhancement of the conduction in 2D materials through a reversible route can significantly improve the signal-to-noise ratio and better contrast in performance at a higher energy efficiency.

In the present work, we use first-principles calculations to study the effect of the proximity of an organic molecule—benzene ($C_6H_6$)—on the transport and electronic properties of an armchair phosphorene nanoribbon (APNR). Benzene lies at the heart of organic chemistry and is widely used in various industries due to its easy availability. Using the nonequilibrium Green's function (NEGF) formalism, the current-voltage characteristics of the APNR are studied in two-probe geometry in the presence and absence of the benzene molecule. Furthermore, we investigate the effect of the system size, doping of varying types (*p* or *n* type), and location on the conductivity response and how it can be tuned using uniaxial strains. Under specific conditions of strain and doping,

*ray@iitp.ac.in

 

an enormous increase (>1500%) in the current signal is observed, indicating the superior enhancement of the conductivity response of phosphorene in the presence of such a molecule. Furthermore, in a realistic FET geometry, we explore how a gate voltage can be used to fine tune the conductivity behavior. We believe that our results will provide detailed insight into the tuning and control of the conductivity of phosphorene in a sub-10-nm structure, shedding light on desirable conditions to unveil the most prudent response that will lead to new possibilities in 2D nanoelectronics.

## II. COMPUTATIONAL DETAILS

First-principles calculations of the electronic structure and geometry relaxation are carried out by self-consistent density-functional theory (DFT) using the Atomistix toolkit (ATK) [34]. The exchange-correlation energy is assessed using the Perdew-Burke-Ernzerhof exchange-correlation functional [35] within the generalized gradient approximation (GGA), where the wave functions are expanded within a double-$\zeta$ polarized basis set under the periodic boundary conditions with an energy-cutoff limit of 180 Ry. The reciprocal space of the Brillouin zone is sampled using a $27 \times 27 \times 1$ Monkhorst-Pack $k$-grid [36]. To reduce the interactions between neighboring layers, a minimum vacuum space of 15 Å is used in the nonperiodic directions. The APNR structures (in pristine and adsorbed conditions) are structurally relaxed until the force on each atom is less than $10^{-3}$ eV/Å, in the equilibrium condition.

All the transport calculations in the two-probe configuration are carried out using the methodology of the NEGF combined with DFT [37,38]. The current is estimated using the Landauer-Büttiker formula [39,40], given by

$$I = \frac{2e}{\hbar}\int_{-eV/2}^{eV/2} T(E,V)[f_L(E-\mu_L) - f_R(E-\mu_R)]dE, \quad (1)$$

where $T(E,V)$ is the transmission function at energy $E$ and bias voltage $V$, $f_{L/R}(E,\mu_{L/R})$ is the Fermi distribution, and $\mu_L$ and $\mu_R$ are the electrochemical potentials of the left and right electrodes, respectively. Details of the methodology used for the calculation of $T(E,V)$ and $\mu_L$ and $\mu_R$ are described in the Supplemental Material [41]. A $k$-point sampling of $(1 \times 1 \times 300)$ is adopted for the transport calculations (300 along the transport direction) as no changes in the transmission are observed beyond this limit.

## III. SYSTEM DESCRIPTION

The unit cell of phosphorene (Fig. 1) has lattice constants $\mathbf{a} = 3.3136$ Å and $\mathbf{b} = 4.3763$ Å, where **a** and **b** are the distances between two consecutive repeating $P$ atoms along the zigzag and armchair directions, respectively [42,43]. The bond length along the zigzag direction

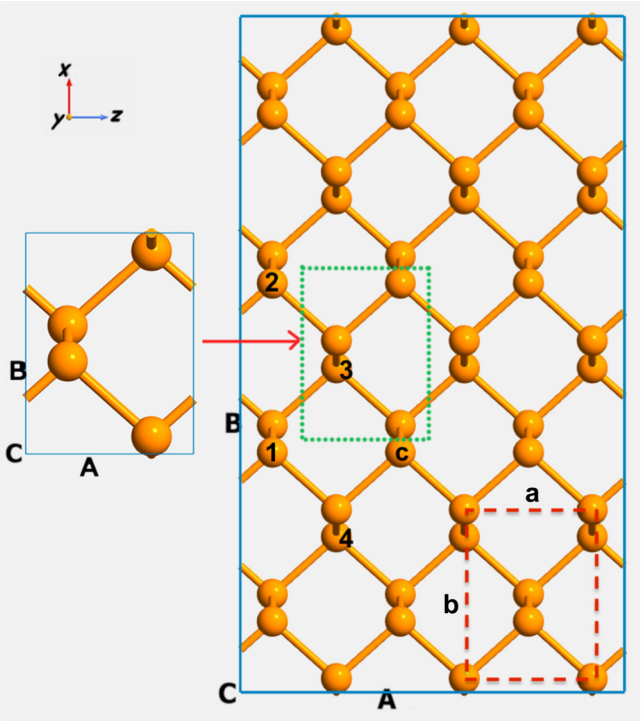


FIG. 1. A schematic of the top view of (left) a unit cell of 2D phosphorene and (right) a $3 \times 4$ supercell of 2D phosphorene, where the two dotted boxes are the unit cells, with **a** and **b** as the lattice vectors. Various doping locations are marked by "C" (center doping) and by "1," "2," "3," and "4" for the locations for edge doping with those numbers of dopant atoms.

containing the in-plane hinge angle of 95.370° is 2.24 Å while the connecting bond length along the armchair direction is 2.26 Å. We designate an $(m \times n)$-sized APNR as $A_{mn}$, with the following dimensions: $m$ times the primitive lattice parameter, **a**, along the zigzag direction and $n$ times the primitive lattice parameter, **b**, along the armchair direction. In the present work, we consider a H-edge passivated $3 \times 4$ supercell of an APNR as our central structure, which is abbreviated as $A_{34P}$ in the pristine structure (no doping and defect) and as $A_{34A}$ in the (benzene-)adsorbed configuration, while $A_{34}$ is adopted for general use.

## IV. RESULTS AND DISCUSSION

### A. The pristine system

The electronic band structure of $A_{34}$ in the unpassivated, passivated, and benzene-adsorbed conditions is illustrated in Fig. 2, which is observed to be a direct-band-gap semiconductor occurring at the Γ point. Compared to the unpassivated system, an increment in band gap is observed from 0.88 eV to 1.24 eV due to H-passivation. The origin of this increment can be traced by comparing the band structures between these two cases. As shown in Fig. 2(b),

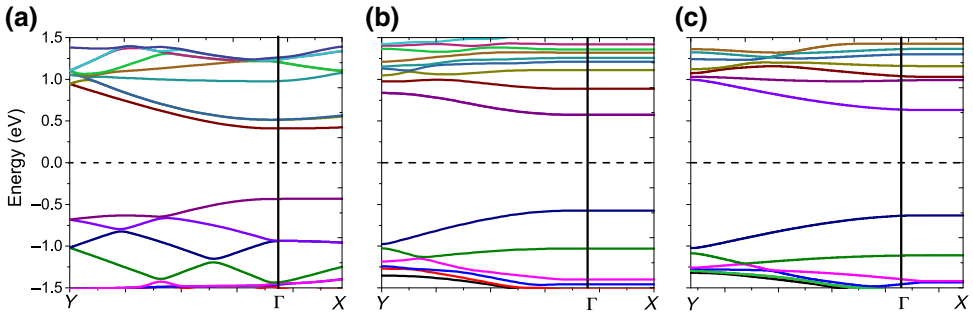


FIG. 2. The band structure of $A_{34}$ in the (a) unpassivated and (b) H-edge passivated configurations and (c) after the adsorption of a benzene molecule.

the valence band shifts downward, whereas the conduction band moves upward in energy after passivation, thus increasing the band gap of $A_{34}$. After adsorbing the benzene molecule, the band gap of $A_{34}$ changes to 1.26 eV [Fig. 2(c)]. This suggests that the semiconducting nature of the APNR remains unaffected through the process of molecular adsorption. The experimentally reported band gap for monolayered phosphorene lies between 0.98 and 1.45 eV [2,5,44], which is comparable to our estimated value. With a change in the band gap, the barrier heights for electrons and holes will vary depending on the relative positions of the conduction and valance bands with respect to the electrodes. Transmission will occur at those energies outside the band gap, depending on the applied bias and the relative positions of Fermi levels of the left and right electrodes.

In order to measure the current-voltage ($I$-$V$) characteristics of $A_{34}$, the central scattering region is connected between two semi-infinite perfect electrodes as shown in Fig. 3(a). In this measurement geometry, the benzene molecule is adsorbed to the side of the APNR. Out of the several configurations tested in this geometry, it is observed that the planar configuration (the molecule and APNR in the same plane) has a lower energy compared to the tilted configuration (molecule remaining at an angle with respect to the APNR) as shown in Fig. S1 of the Supplemental Material [41]. Apart from the side adsorption scenario, we also consider the situation with the molecule adsorbed on top of the layer at various locations. However, the planar configuration as illustrated in Fig. 3(a) is found to be the optimal adsorption configuration and thus considered as the preferred geometry here.

The $I$-$V$ characteristics of $A_{34}$ are shown in Fig. 3(b). At zero bias, no current flows as the density of states in both of the electrodes are identical. A nonzero value of current is observed when the applied bias goes above 0.9 V, which roughly corresponds to the band gap of $A_{34}$. In the presence of the attached molecule, the overall shape of the $I$-$V$ curve shows the characteristics of a gapped structure, as also observed in the pristine case. This agrees well with the trend observed from the band-structure calculations. However, it is noted that attaching the molecule results in a small reduction of current at around 1.2 V and that the difference increases toward higher applied bias. This can be explained as follows: the conduction pathways are lying along the central part and edges of the layer. When the molecule is adsorbed, the local density of electronic states along the conduction paths decreases. Thus the path available for conduction and the transmission get slightly reduced, resulting in a reduced current and conduction. This can be confirmed from the transmission behavior as illustrated in Fig. 3(c), where the value of the transmission in the energy range of −0.5 eV to 0.5 eV is clearly higher for the pristine configuration compared to the adsorbed counterpart. As the $I$-$V$ characteristics in the two cases are significantly different at higher voltages, this suggests that the APNR is sensitive to the presence of such organic objects and that the sensitivity can be measured from the difference of the current(s) at a particular applied bias. A quantitative estimation can be done using the modulation

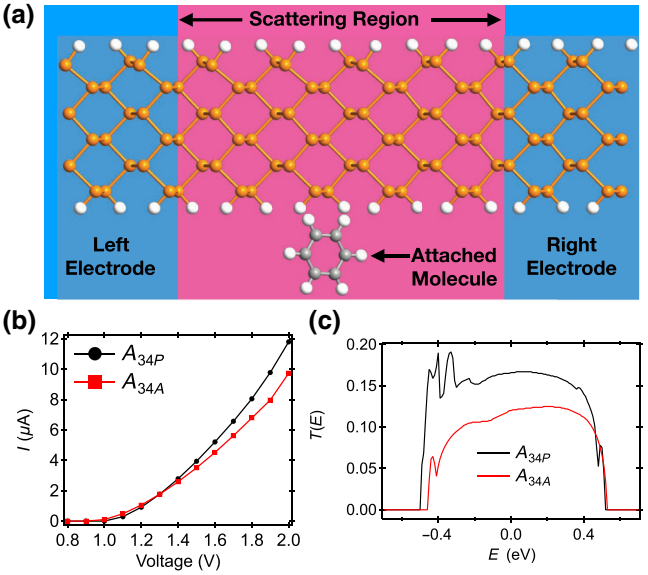


FIG. 3. (a) A schematic of an APNR in two-probe geometry for $I$-$V$ calculations with an attached benzene molecule. (b) The $I$-$V$ relationship of $A_{34}$ in the pristine and adsorbed configurations. (c) The corresponding transmission spectrum at 2.0 V of applied bias.

factor $\eta$, defined at a given bias $V$ as

$$\eta(V) = \left| \frac{I_A(V) - I_U(V)}{I_U(V)} \right| = \left| \frac{\Delta I(V)}{I_U(V)} \right|, \qquad (2)$$

where $I_A$ and $I_U$ are the currents in the adsorbed and unadsorbed configuration of the APNR, respectively.

Next, we check the effect of system size on the electronic and transport properties in the presence of the molecule. The size dependence of the band gap as function of the length $n$ and width $m$ is illustrated in Fig. 4(a). With an increase in width, the band gap gets reduced, which is a consequence of the quantum-confinement effect. On the other hand, the band gap increases with an increase in the length $n$. Also, the bands become flatter (Fig. S2 in the Supplemental Material [41]) as the length increases. This is a result of increased scattering along the ribbon length causing the transmission probability to decrease drastically, which implies an increase in effective mass and hence the flatter bands. However, the band dispersions remain more or less same with the variation of $m$. In both the length and width variation, the band gap for the adsorbed system follows a trend similar to that of its pristine counterpart.

The $I$-$V$ relationships in the adsorbed configuration for various combinations of $m$ and $n$ are illustrated in Fig. 4(b). With an increase in $m$, the current at higher bias becomes enhanced, while the reverse trend is observed with an increase in $n$, i.e., a reduction in current. The highest current is observed when the band gap is the lowest. With an increase in the length of the ribbon, the overall value of the transmission decreases, as also shown in Fig. 4(c). For $A_{34A}$, $A_{54A}$ and $A_{74A}$, a nonzero transmission peak around 0 eV is visible, which almost disappears for $A_{36A}$ and $A_{38A}$. With an increase in $m$, the central window of the transmission remains more or less unchanged, as represented by the dotted lines, but the actual value of the transmission increases manifold at other energies. As the calculated current is the integral sum of transmission, this gets reflected through the $I$-$V$ patterns (current density in Fig. S11 of the Supplemental Material [41]). While the width is kept fixed, the length is increased: the carriers have to travel a longer path and hence the probability of scattering increases and the transmission gets reduced. On the contrary, for a fixed length, an increase in the ribbon width can add additional transmission pathways that can result in an enhanced conduction. While looking at the change in current ($\Delta I$) as a result of the adsorption, a measurable difference is observed for all the configurations tested here, as displayed in Fig. 4(b) (inset). A maximum in $\Delta I \sim 2.7$ $\mu$A is observed for $A_{74P}$, which is about 29.5% higher than the value estimated for $A_{34P}$. Such values of $\Delta I$ are experimentally measurable and are well above the experimental noise floor (approximately in the picoampere range) at room temperature and much higher than the typical values reported for phosphorene [45–47]. In terms of modulation, $\eta \sim 150\%$ is observed for $A_{38P}$, which indicates that a large change in the transport properties of the APNR can be brought about in the presence of the molecule. This property can thus be well utilized for designing a nanosensor made of phosphorene. With a change of the edge structure, it will be interesting to study the behavior of a zigzag nanoribbon under identical circumstances. In earlier works involving graphene nanoribbon, it has been observed that transport behavior gets modulated independent of the edge structures [48]. The shape of the nanoribbon determines the transport pathways for conduction and any modification to this can perturb the other. Passivation of the edge structure offers better stability compared to an unpassivated system due to the saturation of the dangling bonds.

### B. The effect of doping

To check the effect of doping on the electronic and transport properties of the APNR, two different doping strategies are employed. Silicon is used as a $p$-type dopant,

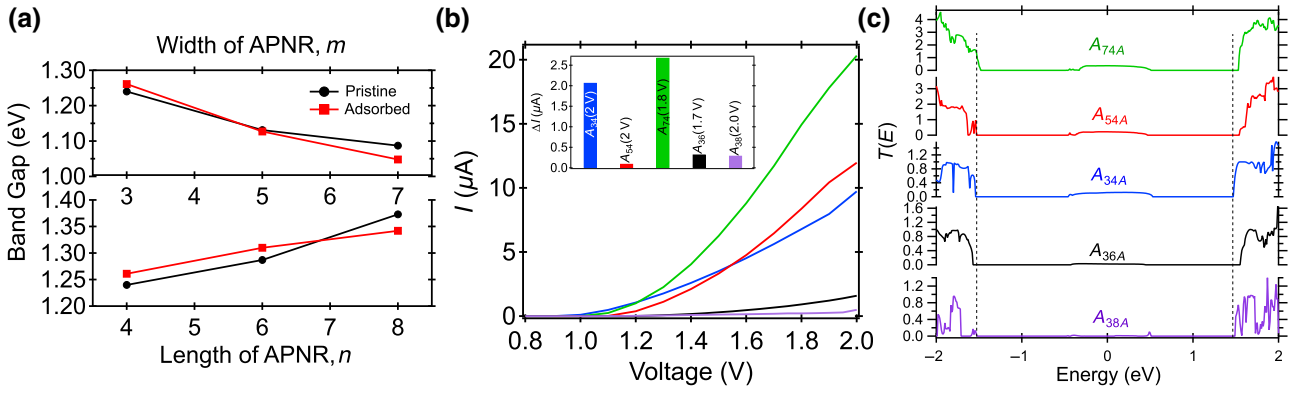


FIG. 4. (a) The dependence of the band gap with length ($n$) and width ($m$) of the APNR in the pristine and adsorbed configurations. (b) The $I$-$V$ relationship of $A_{mn}$ in the adsorbed configuration and (inset) the maximum $\Delta I$ for these cases. (c) The transmission spectrum at 2.0 V applied bias for the respective adsorbed configurations.

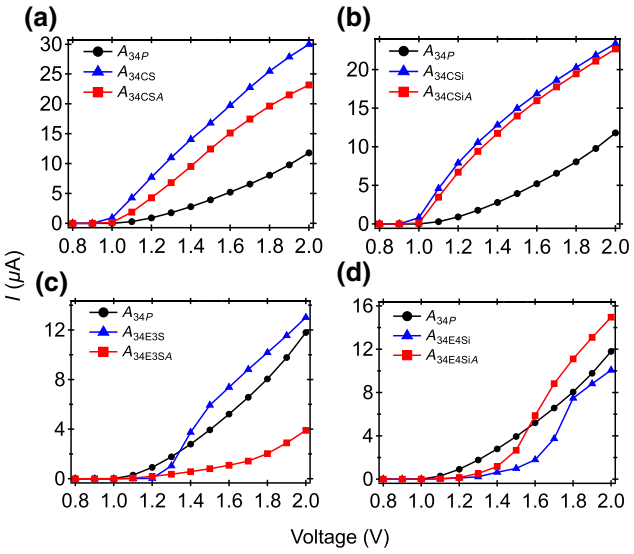


FIG. 5. The $I$-$V$ characteristics of $A_{34}$ in doped configurations: (a) center doped with S, (b) center doped with Si, (c) edge doped with three S atoms, and (d) edge doped with four Si atoms. The red, blue, and black lines represent the undoped, doped, and adsorbed configurations, respectively.

while sulfur is used as an $n$-type dopant. For both types, site-specific doping is performed by placing the dopant atom at the center (center doping) and at the edge (edge doping). In our calculations, the edge-doping concentrations are gradually increased by sequentially replacing the numerically marked sites (see Fig. 1) with one (1.56%), two (3.125%), three (4.59%), and four (6.25%) dopant atoms. They are termed "C" (center doped with one atom) and "E1" to "E4" (edge doped with one to four atoms, respectively). The nomenclature used to define these doping configurations is as follows: $A_{34\mathrm{CSi}}$ represents center doping with Si of $A_{34P}$, while $A_{34\mathrm{CSiA}}$ denotes the same in the adsorbed configuration. Similarly, $A_{34\mathrm{E3S}}$ is used for edge-doped $A_{34P}$ with three S atoms and $A_{34\mathrm{E3SA}}$ for the corresponding adsorbed structure. For $A_{34P}$, edge doping is limited to a maximum of four dopant atoms to prevent doping of the electrodes, which is undesirable. With an increase in the $n$-type doping concentration, the Fermi level shifts downward, whereas for $p$-type doping, the Fermi level shifts toward the higher energies (see Fig. S3 in the Supplemental Material [41]).

The $I$-$V$ curves for $A_{34P}$ center doped with sulfur are illustrated in Fig. 5(a). In all three configurations, significant current starts to flow when the applied bias crosses 0.9 V, which is a signature of a semiconductor with a sizeable band gap. Compared to the pristine configuration, the value of the current remains significantly higher in the doped geometry and the difference becomes enhanced ($\Delta I_{\mathrm{max}} = 18.16\ \mu\mathrm{A}$) with an increase in the bias. In the proximity of the benzene molecule, the $I$-$V$ pattern follows a trend similar to that of the doped case but a marked difference between the two lines is significant for the entire bias region. In this doped configuration, a maximum value of $\eta \sim 83.57\%$ is observed and a maximum of $\Delta I = 6.8\ \mu A$. In a similar manner, the pronounced effect of Si doping at the center can be seen from the $I$-$V$ characteristics in Fig. 5(b). With an increase in the applied bias above the gap size of the APNR, the current in the doped configuration becomes highly enhanced compared to its pristine counterpart, with a maximum of $\Delta I = 10.9\ \mu A$ at 2 V. In the presence of benzene, the difference in the current between the two configurations is clearly visible.

For the edge-doped configuration with three S and four Si atoms, the $I$-$V$ characteristics are shown in Figs. 5(c) and 5(d), respectively. For both types of dopants, the onset voltage $V_{\mathrm{onset}}$ at which finite current starts flowing in the system becomes enhanced in the doped configuration compared to its pristine counterparts. For the Si doping in Fig. 5(d), $V_{\mathrm{onset}} \sim 0.9$ V in the pristine structure, while in the doped geometry, $V_{\mathrm{onset}} \sim 1.2$ V. This trend is present for S doping in Fig. 5(c), but the difference in the onset voltage between the pristine and the doped configuration increases with an increase in the doping percentage. With an increment in the applied bias in Fig. 5(d), current starts rising monotonically in the doped configuration both in the presence and absence of the benzene molecule and a clear difference between the current(s) indicates that edge doping has a more pronounced effect for Si (Fig. S4 in the Supplemental Material [41]). This leads to a huge enhancement $\eta$ of 228.07% and a significant $\Delta I \sim 5\ \mu$A at high voltages.

For S doping at the edge in Fig. 5(c), a pronounced difference in the current is observed as a result of the proximity effect, with $\eta = 569.80\%$ and a maximum of $\Delta I = 9.1\ \mu A$. The large change in the current suggests the influence of the enhanced proximity of the $C_6H_6$ molecule in this APNR. In the edge-doped APNR, additional carriers are locally more available near the edge region, which is in closer proximity to the benzene molecule. This leads to a larger change in the transmission, as shown in Fig. S5 in the Supplemental Material [41]. The disappearance of the transmission peak around the Fermi level in the presence of benzene significantly reduces the integrated sum of $T(E)$ over the entire bias range, leading to a huge reduction of current. For various doping configurations, the values of $\eta$, which are significantly large independent of the doping type and configuration, are tabulated in Table I. The general trend suggests that both $p$- and $n$-type dopants are useful for the conductivity modulation of the APNR. As doping in a semiconductor introduces additional charge carriers for conduction, which for a 2D material with higher surface sensitivity results in an enhanced charge transfer between the layer and the molecule and conductivity changes. To better the value of $\eta$, edge doping is more effective, which for Si increases monotonically with an increase in the doping percentage. This offers additional

TABLE I. A comparison of the maximum conductivity modulation $\eta$ of the APNR in various doping configurations.

| Doping configuration | $\eta$ (Si) | $\eta$ (S) |
|---|---|---|
| C1 (1.56%) | 84.24% (1 V) | 83.57% (1 V) |
| E1 (1.56%) | 39.29% (1.1 V) | 90.77% (1.1 V) |
| E2 (3.13%) | 90.32% (1.1 V) | 142.07% (1.1 V) |
| E3 (4.59%) | 206.44% (1.1 V) | 569.80% (1.2 V) |
| E4 (6.25%) | 228.07% (1.6 V) | 84.94% (1.1 V) |

tuneability in the conduction response in the presence of an organic molecule.

The presence of a benzene molecule has not been found to affect the band structure of the doped APNR (both for Si and S doping). However, the transport properties are affected to a great degree and show varying characteristics depending upon the site and the concentration of doping as the dopant states are induced near the Fermi level of the central scattering region. It is expected that in the case of $A_{34P}$, where the current decreases on adsorption, a similar circumstance will occur for the doped APNR until sufficient delocalized energy states are provided by the dopant atoms and in our study we also observe a similar situation. We note a decrement in the current after adsorption of a benzene molecule when the APNR is doped with up to two Si atoms; but when the system is doped with three and four Si atoms, respectively, the current increases after the adsorption of a benzene molecule. On the other hand, for a sulfur-doped APNR, a fall in current is observed when the system is doped with one S atom (both center and edge doped) and a rise in current is observed after the system is doped with two or four S atoms, in accordance with our expectations.

In the pristine configuration, a center-doped APNR clearly transports a higher magnitude of current than the other doped ribbons. This is due to the fact that in an H-edge passivated APNR, the H—P bonds are stronger and the edge states are located deep in the bands [12]. The CBM (conduction-band minima) and the VBM (valance-band maximum) are contributed by the atoms in the central region, while centrally doped Si creates a dopant state in the Fermi level. Consequently, the major part of the current flows through the central pathways, as also observed from the transmission analysis. Henceforth, to magnify the current values further, the delocalized states created by the centrally doped Si are preferable compared to the edge-doped configurations.

### C. The influence of strain

To investigate the influence of external strain on the conductivity of the APNR, electronic and transport properties are studied in the pristine and adsorbed configurations. The percentage uniaxial strain is defined using the following equation: $S = 100\% \times (a - a_0)/a_0$, where $a_0(a)$ is the lattice constant in the unstrained (strained) configuration of the APNR. In this work, we cover a significantly large strain range of $S = -15\%$ to $+15\%$. Within this region of strain, the gap size of the APNR stays within a range of 0.8–1.3 eV (Fig. S6 in the Supplemental Material [41]). In the adsorbed condition, no major changes in the band gap are observed except for a small difference at $S = 6\%$. This suggests that the semiconducting nature of the material does not get affected on benzene adsorption in the strained configuration. The APNR is found to be stable within the elastic limit for a maximum applied strain of $S = 30\%$.

The semiconducting nature of the APNR is visible from the $I$-$V$ behavior of $A_{34P}$ at $S = 2\%$, as shown in Fig. 6(a). On adsorption, the current starts flowing at a much smaller bias compared to $A_{34P}$ and above 1.45 V the current traces a path similar to that of its pristine counterpart. At $S = 6\%$, the differences in the $I$-$V$ characteristics in Fig. 6(b) between the pristine and adsorbed configurations are much more pronounced over the entire range of applied bias. In the adsorbed configuration, above 0.2 V, current starts to increase with an increase in the applied bias, with a current peak at 1.36 V followed by a minimum at 1.6 V—above which, it increases sharply at higher voltages. These kinds of conductance oscillations have been observed in phosphorene and other 2D materials [48,49] and can be explained using the changes in the transmission behavior as shown in Fig. S7 in the Supplemental Material [41]. Similar peak and valley regions are weakly visible in the pristine configuration, but the overall amplitude of the current oscillations is relatively less. In the compressive strain region [Figs. 6(c) and 6(d)], the gapped electronic structure of the APNR is noticeable from the $I$-$V$ responses and the current in the adsorbed configuration is lower than the pristine configuration over the entire bias range. This is in contrast to the tensile strain regime, where the current becomes enhanced on adsorption.

Here, it is observed that with an increase in the applied strain (in tensile and compressive regimes), the APNR starts conducting at a lower voltage than the unstrained APNR in both the absorbed and unabsorbed configurations. For $S = 6\%$, nonzero current is measured at 0.2 V and for both $S = 10\%$ and 14% conduction starts at an astonishingly small bias of 0.1 V), in spite of having a larger band gap. A similar trend is observed in the compressive strain region, where for $S = -6\%$, the current starts flowing at 0.1 V for the pristine case. This disparity in the relation between a large band gap and a low bias voltage for conducting current is the consequence of the electrodes becoming semimetallic when strained. The reason for this can be explained in the following way. Under the application of an in-plane strain, the layer gets stretched horizontally. This enhances the in-plane bond

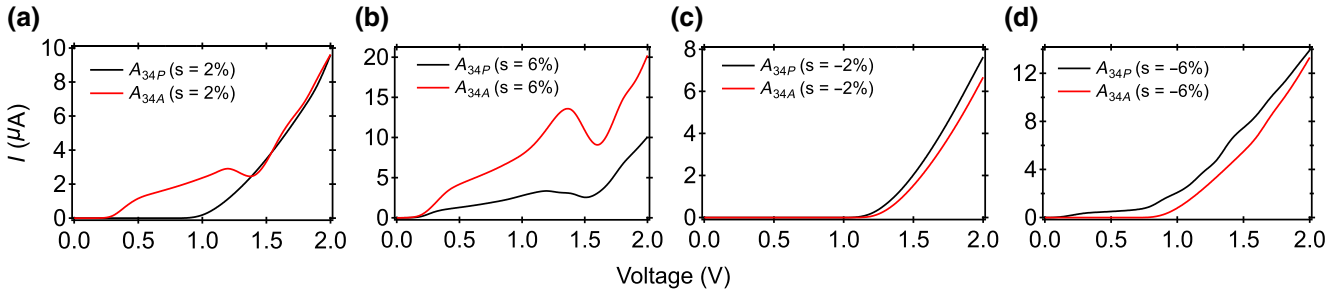


FIG. 6. The $I$-$V$ response of $A_{34}$ in the pristine and adsorbed configurations under (a) 2%, (b) 6%, (c) −2%, and (d) −6% applied strain.

length between the P atoms and brings about a reduction of the out-of-plane bond length. As a result, the overlap of the $3p_x$ and $3p_y$ orbitals between neighboring P atoms gets reduced, while the $3p_z$ contribution becomes enhanced in the respective cases. When the in-plane lattice sites are widely separated, this diminishes the scattering probability by increasing the scattering time due to this reduced orbital overlap. This results in the current hike when the applied strain is increased up to a certain level. In the compressive-strain region, the hopping probability becomes enhanced with a higher degree of overlap between the $3p_x$ and $3p_y$ orbitals, which can explain the onset of the current at lower bias.

The conductivity changes obtained for different strain configurations are listed in Table II and are significantly large for the entire region of strain studied here. Overall, $\eta$ is higher in the tensile regime compared to the compressive cases. At $S = 2\%$, a colossal value of $\eta = 1527.8\%$ is observed, which on enhancement of the tensile strain stays high, with a value of 365.44% at $S = 6\%$. Within the Landauer's formalism, such a high value of $\eta$ can be explained by comparing the transmission behavior in the pristine and adsorbed cases as illustrated in Fig. S8 in the Supplemental Material [41] for $S = 2\%$ at 1 V of applied bias. Between the energy ranges of $-0.46$ eV $\rightarrow$ $-1.07$ eV and 0.87 eV $\rightarrow$ 1.02 eV, transmission is mostly absent in the pristine system, while it is nonzero for the adsorbed case. Compared to the pristine case, $T(E)$ is significantly higher for the adsorbed case up to an energy of $-1.5$ eV. Similar differences in transmission is also observed for $S = 6\%$ at 1.5 V of applied bias (Fig. S9 in the Supplemental Material [41]), which explains the origin of the high value of $\eta$ for these cases. The value of $\eta$ in the compressive-strain regime stays over 80% up to $S = -10\%$. Such an unprecedented level of conductivity modulation has not been observed in phosphorene before, which suggests that the application of strain can be a very effective way of achieving enhanced conduction in phosphorene.

TABLE II. A comparison of the maximum conductivity modulation $\eta$ of the APNR at various values of the applied strain (in %).

| Strain | $\eta$ | Strain | $\eta$ |
|---|---|---|---|
| 2% | 1527.81 (1.0 V) | −2% | 85.90 (1.2 V) |
| 6% | 365.44 (1.5 V) | −6% | 86.77 (0.9 V) |
| 10% | 232.5 (0.2 V) | −10% | 81.59 (0.8 V) |
| 14% | 70.32 (1.1 V) | −14% | 42.85 (0.1 V) |

### D. The effect of a gate voltage

To understand the influence of the gate voltage on the conductance behavior, the transport properties of the APNR are studied in a FET geometry, as illustrated in Fig. 7(a). The structure consists of a metallic gate connecting the APNR through a dielectric layer. The dielectric constant is taken as $\epsilon_r = 4.2$, which is similar to that of $SiO_2$, commonly used in FETs. In this all-phosphorene FET, the source ($S$) and drain ($D$) electrodes are also considered to be made of phosphorene, which rules out the presence of barriers at the metal-semiconductor interfacial contacts and their effects on transport properties.

In the presence of a $V_g$, the $I$-$V$ pattern retains the semiconducting character of the APNR in the FET structure, as can be seen in Fig. 7(b). At $V_g = 20$ V, a pronounced difference in the current can be observed between the pristine and the adsorbed configuration that results in an extreme $\eta \sim 300\%$, which, at $V_g = 10$ V, also stays very high at 200%. Within a large $V_g$ range of $-20$ V to $+20$ V, the $I$-$V$ characteristics in the adsorbed configurations are illustrated in Fig. 7(c). With an increase in the bias, the difference in the current becomes enhanced which is maximum at $V_g = 10$ V, $-10$ V with a maximum $\Delta I \sim 36.5$ $\mu$A. At higher values of $V_g = 20$ V, $-20$ V, it is also significantly large at 26 $\mu$A at 2 V applied bias. First, the presence of such a large current (approximately 45 $\mu$A) at both positive and negative values of $V_g$ confirms that the ambipolar nature of the APNR remains intact in the adsorbed configuration. Second, the transverse electric field of the gate voltage offers a better enhancement of

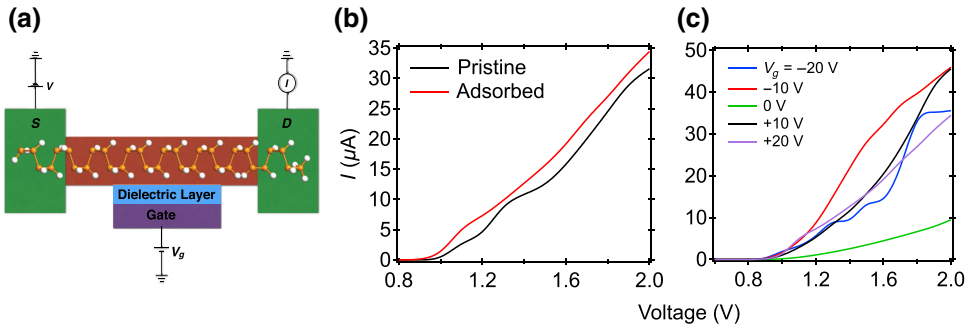


FIG. 7. (a) An APNR-based FET structure with a back gate. (b) The $I$-$V$ characteristics of $A_{34}$ at $V_g = 20$ V in the pristine and adsorbed configurations. (c) The $I$-$V$ response in the adsorbed configuration ($A_{34A}$) at various values of $V_g$ ($S$, source; $D$, drain).

current in the adsorbed configuration compared to its pristine counterpart. This indicates the effect of the presence of a benzene molecule on the conduction behavior of the APNR. The large change in the current due to a change of $V_g$ suggests that a back gate can control the conduction response in a reversible manner without bringing about permanent changes in the material.

Apart from the configuration discussed in this work, the conductance modulation is observed irrespective of the adsorption configuration considered from the top or side of the nanoribbon. This effect is present under the influence of various external influences, such as (a) the application of strain, (b) the presence of dopants of various types at different locations, and (c) the inclusion of a gate voltage, the conductivity enhancement is present against various external fluctuations, which is unlike an observation made at a specific condition. On the basis of the observed trend, it is expected that multiple adsorption of molecules will lead to a much larger change in conductivity in such an APNR.

As the width of the APNR grows, the changes in conductance can be reduced. However, the effect is expected to smear only for large flakes in the micron width range, while for nanoribbons of technological interest having widths of a few nanometers, the changes are still expected to be significant. Experimentally, nanoribbons of similar dimension in 2D crystals have already been grown using multiple routes [50], in lateral heterostructures [51], vertical stacks [52], and from a liquid precursor [53]. The introduction of nanoscale defects [54,55] with atomic-scale uniformity and long-range order in such 2D structures has been demonstrated. In addition, scanning-tunneling-microscope (STM) based lithography techniques [51,56,57] have been useful in generating preferred edge structures and in the detection of attached molecules in a nanoribbon. Strain can be applied using a bending apparatus, by nanoindentation in an atomic-force microscope, or through the use of flexible substrates [10]. Single-molecule detection has been experimentally observed for graphene [29,58] and carbon nanotube [59,60], where decreasing the channel length led to an increase in the sensitivity up to a critical dimension, as considered in the present work. These reports suggest the possibility of creating nanoribbons of current interest, especially with STM-based local oxidation. Such a prospect makes our work as a useful guideline for future experiments.

## V. CONCLUSION

In this work, first-principles based nonequilibrium Green's function (NEGF)–density-functional theory (DFT) calculations are used to investigate the electronic and transport properties of a phosphorene nanoribbon in the close proximity of an organic molecule and to detect a supreme modulation of the conduction response. We observe that in the absence of any external stimuli, the conduction behavior changes significantly in the presence of the molecule, while the semiconducting nature of phosphorene remains similar. The conduction modulation is characterized by a modulation parameter $\eta$, which has a maximum of approximately 150% in this environment. We observe that the behavior can be further controlled by (i) doping, (ii) applying strain, and (iii) applying a gate voltage. Independent of the doping type, location, and concentration, a paramount amount of change was observed with a maximum $\eta \sim$ 570% with edge-doped sulfur. On the other hand, under the application of strain, a colossal enhancement of the current and $\eta \sim 1528\%$ was measured under 2% tensile strain. The gate voltage offers controlled tuning of this effect with a maximum conduction change $\eta \sim 300\%$ in a noninvasive manner. Due to the larger values of the measured currents (20–50 $\mu$A) and a gate-controlled conductivity modulation of almost 400% ($\Delta V_g = 10$ V) in the adsorbed configuration, the feasibility of practical studies is significantly high, thanks to the advancement of the present-day nanotechnological tools. The conductivity modulation will be prevalent for nanoribbons with a size of a few nanometers, as commonly required for the fabrication of a semiconducting channel in a present-day electronic device, compared to that of a much wider nanoribbon with larger numbers of central transport pathways. Our current findings provide insight into proximity-induced tuning and control of the conduction response of phosphorene and propose direction for its usefulness in various nanoscale applications in switching, superior sensing [61,62], and energy-efficient designs, and so on.

## ACKNOWLEDGMENTS

This work was financially supported by Department of Science and Technology, Government of India through the INSPIRE scheme (Grant No. DST/INSPIRE/04/2015/003087).



[1] K. S. Novoselov, D. Jiang, F. Schedin, T. J. Booth, V. V. Khotkevich, S. V. Morozov, and A. K. Geim, Two-dimensional atomic crystals, PNAS **102**, 10451 (2005).

[2] Saptarshi Das, Wei Zhang, Marcel Demarteau, Axel Hoffmann, Madan Dubey, and Andreas Roelofs, Tunable transport gap in phosphorene, Nano Lett. **14**, 5733 (2014).

[3] Gen Long, Denis Maryenko, Junying Shen, Shuigang Xu, Jianqiang Hou, Zefei Wu, Wing Ki Wong, Tianyi Han, Jiangxiazi Lin, Yuan Cai, Rolf Lortz, and Ning Wang, Achieving ultrahigh carrier mobility in two-dimensional hole gas of black phosphorus, Nano Lett. **16**, 7768 (2016).

[4] Likai Li, Yijun Yu, Guo Jun Ye, Qingqin Ge, Xuedong Ou, Hua Wu, Donglai Feng, Xian Hui Chen, and Yuanbo Zhang, Black phosphorus field-effect transistors, Nat. Nanotechnol. **9**, 372 (2014).

[5] Han Liu, Adam T Neal, Zhen Zhu, Zhe Luo, Xianfan Xu, David Tomnek, and Peide D. Ye, Phosphorene: An unexplored 2D semiconductor with a high hole mobility, ACS Nano **8**, 4033 (2014).

[6] Ahmet Avsar, Jun Y. Tan, Marcin Kurpas, Martin Gmitra, Kenji Watanabe, Takashi Taniguchi, Jaroslav Fabian, and Barbaros Ozyilmaz, Gate-tunable black phosphorus spin valve with nanosecond spin lifetimes, Nat. Phys. **13**, 888 (2017).

[7] M. Venkata Kamalakar, B. N. Madhushankar, Andre Dankert, Saroj P. Dash, Low Schottky barrier black phosphorus field-effect devices with ferromagnetic tunnel contacts, Small **11**, 2209 (2015).

[8] Ruixiang Fei and Li Yang, Strain-engineering the anisotropic electrical conductance of few-layer black phosphorus, Nano Lett. **14**, 2884 (2014).

[9] A. S. Rodin, A. Carvalho, and A. H. Castro Neto, Strain-Induced Gap Modification in Black Phosphorus, Phys. Rev. Lett. **112**, 176801 (2014).

[10] S. J. Ray and M. Venkata Kamalakar, Unconventional strain-dependent conductance oscillations in pristine phosphorene, Phys. Chem. Chem. Phys. **20**, 13508 (2018).

[11] Jie Guan, Zhen Zhu, and David Tomanek, Phase Coexistence and Metal-Insulator Transition in Few-Layer Phosphorene: A Computational Study, Phys. Rev. Lett. **113**, 046804 (2014).

[12] Qingyun Wu, Lei Shen, Ming Yang, Yongqing Cai, Zhigao Huang, and Yuan Ping Feng, Electronic and transport properties of phosphorene nanoribbons, Phys. Rev. B **92**, 035436 (2015).

[13] Mohammad Elahi, Kaveh Khaliji, Seyed Mohammad Tabatabaei, Mahdi Pourfath, and Reza Asgari, Modulation of electronic and mechanical properties of phosphorene through strain, Phys. Rev. B **91**, 115412 (2015).

[14] Xihong Peng, Qun Wei, and Andrew Copple, Strain-engineered direct-indirect band gap transition and its mechanism in two-dimensional phosphorene, Phys. Rev. B **90**, 085402 (2014).

[15] Xiaoyu Han, Henry Morgan Stewart, Stephen A. Shevlin, C. Richard, A. Catlow, and Zheng Xiao Guo, Strain and orientation modulated bandgaps and effective masses of phosphorene nanoribbons, Nano Lett. **14**, 4607 (2014).

[16] Qun Wei and Xihong Peng, Superior Mechanical Flexibility of Phosphorene and Few-Layer Black Phosphorus, Appl. Phys. Lett. **104**, 251915 (2014).

[17] Jin-Wu Jiang and Harold S. Park, Negative Poisson's ratio in single-layer black phosphorus, Nat. Commun. **5**, 4727 (2014).

[18] Zhen Zhu and David Tomanek, Semiconducting Layered Blue Phosphorus: A Computational Study, Phys. Rev. Lett. **112**, 176802 (2014).

[19] Deniz Cakir, Hasan Sahin, and Francois M. Peeters, Tuning of the electronic and optical properties of single-layer black phosphorus by strain, Phys. Rev. B **90**, 205421 (2014).

[20] Hongyan Guo, Ning Lu, Jun Dai, Xiaojun Wu, and Xiao Cheng Zeng, Phosphorene nanoribbons, phosphorus nanotubes, and van der Waals multilayers, J. Phys. Chem. C **118**, 14051 (2014).

[21] Yan Li, Shengxue Yang, and Jingbo Li, Modulation of the electronic properties of ultrathin black phosphorus by strain and electrical field, J. Phys. Chem. C **118**, 23970 (2014).

[22] Jingsi Qiao, Xianghua Kong, Zhi-Xin Hu, Feng Yang, and Wei Ji, High-mobility transport anisotropy and linear dichroism in few-layer black phosphorus, Nat. Commun. **5**, 4475 (2014).

[23] A. N. Rudenko and M. I. Katsnelson, Quasiparticle band structure and tight-binding model for single and bilayer black phosphorus, Phys. Rev. B **89**, 201408 (2014).

[24] Vy Tran, Ryan Soklaski, Yufeng Liang, and Li Yang, Layer-controlled band gap and anisotropic excitons in few-layer black phosphorus, Phys. Rev. B **89**, 235319 (2014).

[25] Jun Dai and Xiao Cheng Zeng, Bilayer phosphorene: Effect of stacking order on bandgap and its potential applications in thin-film solar cells, J. Phys. Chem. Lett. **5**, 1289 (2014).

[26] Yongqing Cai, Gang Zhang, and Yong-Wei Zhang, Layer-dependent band alignment and work function of few-layer phosphorene, Sci. Rep. **4**, 6677 (2014).

[27] Can Wang, Qinglin Xia, Yaozhuang Nie, and Guanghua Guo, Strain-induced gap transition and anisotropic Dirac-like cones in monolayer and bilayer phosphorene, J. Appl. Phys. **117**, 124302 (2015).

[28] Ruixiang Fei, Vy Tran, and Li Yang, Topologically protected dirac cones in compressed bulk black phosphorus, Phys. Rev. B **91**, 195319 (2015).

[29] F. Schedin, A. K. Geim, S. V. Morozov, E. W. Hill, P. Blake, M. I. Katsnelson, and K. S. Novoselov, Detection of individual gas molecules adsorbed on graphene, Nat. Mater. **6**, 652 (2007).

[30] S. Rani and S. J. Ray, Detection of gas molecule using $C_3N$ island single electron transistor, Carbon **144**, 235 (2019).

[31] S. J. Ray and R. Chowdhury, Double gated single molecular transistor for charge detection, J. Appl. Phys. **116**, 034307 (2014).

[32] S. J. Ray, Single atom impurity in a single molecular transistor, J. Appl. Phys. **116**, 154302 (2014).

[33] S. J. Ray, Single molecule transistor based nanopore for the detection of nicotine, J. Appl. Phys. **116**, 244307 (2014).
[34] ATOMISTIX TOOLKIT, Quantum Wise Division.
[35] John Perdew, Kieron Burke, and Matthias Ernzerhof, Generalized Gradient Approximation Made Simple, Phys. Rev. Lett. **77**, 3865 (1996).
[36] Hendrik J. Monkhorst and James D. Pack, Special points for Brillouin-zone integrations, Phys. Rev. B **13**, 5188 (1976).
[37] Jose M. Soler, Emilio Artacho, Julian D. Gale, Alberto Garcia, Javier Junquera, Pablo Ordejon, and Daniel Sanchez-Portal, The SIESTA method for *ab initio* order-*n* materials simulation, J. Phys.: Condens. Matter **14**, 2745 (2002).
[38] Mads Brandbyge, Jose-Luis Mozos, Pablo Ordejon, Jeremy Taylor, and Kurt Stokbro, Density-functional method for nonequilibrium electron transport, Phys. Rev. B **65**, 165401 (2002).
[39] R. Landauer, Spatial variation of currents and fields due to localized scatterers in metallic conduction, IBM J. Res. Dev. **32**, 306 (1988).
[40] M. Buttiker, Y. Imry, R. Landauer, and S. Pinhas, Generalized many-channel conductance formula with application to small rings, Phys. Rev. B **31**, 6207 (1985).
[41] A. Chaudhury *et al.*, See the Supplemental Material at http://link.aps.org/supplemental/10.1103/PhysRevApplied.11.024056 for additional information on Proximity-Induced Colossal Conductivity Modulation in Phosphorene.
[42] S. J. Ray, First-principles study of $MoS_2$, phosphorene and graphene based single electron transistor for gas sensing applications, Sens. Actuators, B **222**, 492 (2016).
[43] S. J. Ray, M. Venkata Kamalakar, and R. Chowdhury, *Ab-initio* studies of phosphorene island single electron transistor, J. Phys.: Condens. Matter **28**, 195302 (2016).
[44] Xiaomu Wang, Aaron M. Jones, Kyle L. Seyler, Vy Tran, Yichen Jia, Huan Zhao, Han Wang, Li Yang, Xiaodong Xu, and Fengnian Xia, Highly anisotropic and robust excitons in monolayer black phosphorus, Nat. Nanotechnol. **10**, 517 (2015).
[45] Liangzhi Kou, Thomas Frauenheim, and Changfeng Chen, Phosphorene as a superior gas sensor: Selective adsorption and distinct *I-V* response, J. Phys. Chem. Lett. **5**, 2675 (2014).
[46] Yuehua Xu, Jun Dai, and Xiao Cheng Zeng, Electron-transport properties of few-layer black phosphorus, J. Phys. Chem. Lett. **6**, 1996 (2015).
[47] Ajanta Maity, Akansha Singh, Prasenjit Sen, Aniruddha Kibey, Anjali Kshirsagar, and Dilip G. Kanhere, Structural electronic mechanical and transport properties of phosphorene nanoribbons: Negative differential resistance behavior, Phys. Rev. B **94**, 075422 (2016).
[48] R. Chowdhury, S. Adhikari, P. Rees, S. P. Wilks, and F. Scarpa, Graphene-based biosensor using transport properties, Phys. Rev. B **83**, 045401 (2011).
[49] V. Hung Nguyen, F. Mazzamuto, J. Saint-Martin, A. Bournel, and P. Dollfus, Giant Effect of Negative Differential Conductance in Graphene Nanoribbon *p-n* Heterojunctions, Appl. Phys. Lett. **99**, 042105 (2011).
[50] Xuesong Li, Weiwei Cai, Jinho An, Seyoung Kim, Junghyo Nah, Dongxing Yang, Richard Piner, Aruna Velamakanni, Inhwa Jung, Emanuel Tutuc, K. Banerjee Sanjay, Luigi Colombo, and Rodney S. Ruoff, Large-area synthesis of high-quality and uniform graphene films on copper foils, Science **324**, 1312 (2009).
[51] P. Sutter, R. Cortes, J. Lahiri, and E. Sutter, Interface formation in monolayer graphene–boron nitride heterostructures, Nano Lett. **12**, 4869 (2012).
[52] Zheng Liu, Li Song, Shizhen Zhao, Jiaqi Huang, Lulu Ma, Jiangnan Zhang, Jun Lou, and Pulickel M. Ajayan, Direct growth of graphene/hexagonal boron nitride stacked layers, Nano Lett. **11**, 2032 (2011).
[53] Anchal Srivastava, Charudatta Galande, Lijie Ci, Li Song, Chaitra Rai, Deep Jariwala, Kevin F. Kelly, and Pulickel M. Ajayan, Novel liquid precursor-based facile synthesis of large-area continuous, single, and few-layer graphene films, Chem. Mater. **22**, 3457 (2010).
[54] Cesar Moreno, Manuel Vilas-Varela, Bernhard Kretz, Aran Garcia-Lekue, Marius V. Costache, Markos Paradinas, Mirko Panighel, Gustavo Ceballos, Sergio O. Valenzuela, Diego Pena, and Aitor Mugarza, Bottom-up synthesis of multifunctional nanoporous graphene, Science **360**, 199 (2018).
[55] Maxim Ziatdinov, Shintaro Fujii, Koichi Kusakabe, Manabu Kiguchi, Takehiko Mori, and Toshiaki Enoki, Visualization of electronic states on atomically smooth graphitic edges with different types of hydrogen termination, Phys. Rev. B **87**, 115427 (2013).
[56] Levente Tapaszto, Gergely Dobrik, Philippe Lambin, and Laszlo P. Biro, Tailoring the atomic structure of graphene nanoribbons by scanning tunnelling microscope lithography, Nat. Nanotechnol. **3**, 397 (2008).
[57] Donna M. Cyr, Bhawani Venkataraman, George W. Flynn, Andrew Black, and George M. Whitesides, Functional group identification in scanning tunneling microscopy of molecular adsorbates, J. Phys. Chem. **100**, 13747 (1996).
[58] Nihar Mohanty and Vikas Berry, Graphene-based single-bacterium resolution biodevice and dna transistor: Interfacing graphene derivatives with nanoscale and microscale biocomponents, Nano Lett. **8**, 4469 (2008).
[59] Xuefeng Guo, Joshua P. Small, Jennifer E. Klare, Yiliang Wang, Menin-der S. Purewal, Iris W. Tam, Byung Hee Hong, Robert Caldwell, Limin Huang, Ronald Breslow, Shalom J. Wind, James Hone, Philip Kim, and Colin Nuckolls, Covalently bridging gaps in single-walled carbon nanotubes with conducting molecules, Science **311**, 356 (2006).
[60] Brett R. Goldsmith, John G. Coroneus, Vaikunth R. Khalap, Alexander A. Kane, Gregory A. Weiss, and Philip G. Collins, Conductance-controlled point functionalization of single-walled carbon nanotubes, Science **315**, 77 (2007).
[61] S. J. Ray, Single molecular transistor as a superior gas sensor, J. Appl. Phys. **118**, 034303 (2015).
[62] S. J. Ray, Humidity sensor using a single molecular transistor, J. Appl. Phys. **118**, 044307 (2015).
[63] K. Stokbro, J. Taylor, M. Brandbyge, and H. Guo, *Ab-initio Non-Equilibrium Green's Function Formalism for Calculating Electron Transport in Molecular Devices* (Springer, Berlin, Heidelberg, 2005), p. 117–151.
[64] Supriyo Datta, *Electronic Transport in Mesoscopic Systems, Cambridge Studies in Semiconductor Physics and*

*Microelectronic Engineering* (Cambridge University Press, Cambridge, UK, 1995).

[65] Mads Brandbyge, Jose-Luis Mozos, Pablo Ordejon, Jeremy Taylor, and Kurt Stokbro, Density-functional method for nonequilibrium electron transport, Phys. Rev. B **65**, 165401 (2002).

[66] Taisuke Ozaki, Kengo Nishio, and Hiori Kino, Efficient implementation of the nonequilibrium Green function method for electronic transport calculations, Phys. Rev. B **81**, 035116 (2010).

[67] Daniele Stradi, Umberto Martinez, Anders Blom, Mads Brandbyge, and Kurt Stokbro, General atomistic approach for modeling metal-semiconductor interfaces using density functional theory and nonequilibrium Green's function, Phys. Rev. B **93**, 155302 (2016).

[68] Dan Erik Petersen, Hans Henrik B. Srensen, Per Christian Hansen, Stig Skelboe, and Kurt Stokbro, Block tridiagonal matrix inversion and fast transmission calculations, J. Comput. Phys. **227**, 3174 (2008).